

MUSE-VAE: Multi-Scale VAE for Environment-Aware Long Term Trajectory Prediction

Mihee Lee
Rutgers University
USA
ml1323@rutgers.edu

Samuel S. Sohn
Rutgers University
USA
samuel.sohn@rutgers.edu

Seonghyeon Moon
Rutgers University
USA
sm2062@cs.rutgers.edu

Sejong Yoon
The College of New Jersey
USA
yoons@tcnj.edu

Mubbasir Kapadia
Rutgers University
USA
mubbasir.kapadia@rutgers.edu

Vladimir Pavlovic
Rutgers University
USA
vladimir@cs.rutgers.edu

Abstract

Accurate long-term trajectory prediction in complex scenes, where multiple agents (e.g., pedestrians or vehicles) interact with each other and the environment while attempting to accomplish diverse and often unknown goals, is a challenging stochastic forecasting problem. In this work, we propose MUSE-VAE, a new probabilistic modeling framework based on a cascade of Conditional VAEs, which tackles the long-term, uncertain trajectory prediction task using a coarse-to-fine multi-factor forecasting architecture. In its Macro stage, the model learns a joint pixel-space representation of two key factors, the underlying environment and the agent movements, to predict the long and short term motion goals. Conditioned on them, the Micro stage learns a fine-grained spatio-temporal representation for the prediction of individual agent trajectories. The VAE backbones across the two stages make it possible to naturally account for the joint uncertainty at both levels of granularity. As a result, MUSE-VAE offers diverse and simultaneously more accurate predictions compared to the current state-of-the-art. We demonstrate these assertions through a comprehensive set of experiments on nuScenes and SDD benchmarks as well as PFSD, a new synthetic dataset, which challenges the forecasting ability of models on complex agent-environment interaction scenarios.

1. Introduction

Human behavior forecasting is an essential problem studied in various research fields such as computer vision [15], computer graphics [16], robotics [11], and cognitive science [49]. The fundamental problem with predicting human motion is the inherent stochasticity stemming

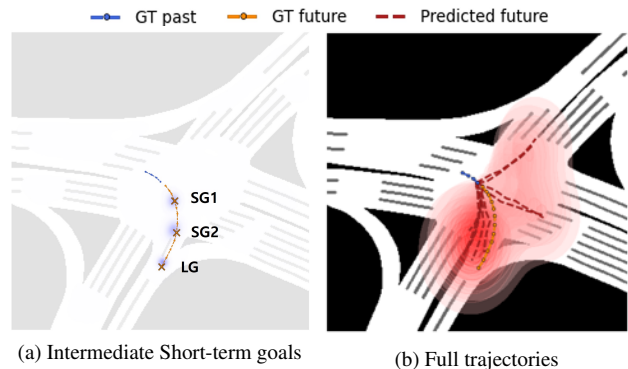


Figure 1. (a) The predicted trajectory heatmaps are overlaid in the semantic map. Ground Truth (GT) long-term goal (LG) and short-term goals (SG1 and SG2) are marked with 'x'. (b) Complete trajectory forecasting based on the predicted LG and SG. Each sequence of trajectories is obtained from a different pair of LG and SG predictions.

from the fact that human beings use numerous sources of information to make a wide variety of different decisions at any given moment, which all impact their future movement. This movement uncertainty translates beyond the motion of the humans alone to the movement of objects controlled by humans, such as vehicles [6].

To embrace the uncertainty, in this paper, we focus on developing computational models, learned from data, that can predict a realistic multi-modal distribution of the future agent (humans, vehicles, etc.) trajectories. The models are designed in the context of two main factors that drive this uncertainty: the environment the agents occupy and the task they are attempting to accomplish.

However, direct forecasting of long-term trajectories is a challenging task. A person typically plans one's movement in a coarse-to-fine fashion: with a final destina-

tion in mind, through a sequence of intermediate goals or way-points, the movement is executed to reach those sub-goals [8, 39]. State-of-the-Art (SOTA) methods [29, 48, 51] leverage this intuition to propose goal-conditioned prediction model. However, despite their effectiveness compared to traditional approaches [1, 15, 47], these models show limited ability to deal with complex environments [48], particularly as they affect the movement [51]. This often results in physically implausible trajectory predictions that violate agent-environment collision constraints. Moreover, the models frequently struggle to account for the diversity of the forecast goals and trajectories [29], which are driven by the uncertain, multi-modal nature of the problem.

To address this, we propose MUSE-VAE: a multi-scale, environment-aware model for long-term trajectory prediction which (1) takes a stage-wise, coarse-to-fine approach to trajectory prediction by predicting both the higher-level goals and the goal-conditioned trajectory, (2) avoids collision with obstacles without loss of spatial signal which can occur due to spatial reorganization when compressing 2D information into 1D features, and (3) learns a multimodal predictive distribution across the stages, thus capturing the inherent uncertainty. MUSE-VAE embodies a three-step learning strategy across a Macro-stage and Micro-stage. The Macro-stage comprises of two steps for coarse predictions. We first predict the long-term goal, i.e., the last step of the given sequence based on heatmap trajectory representation. Given the long-term goal, two sequential short-term goals are predicted as shown in Fig. 1a. After getting the goal positions in the Macro-stages, finally, our model produces the full trajectories in the Micro-stage as in Fig. 1b. Our main contributions are as follows: (a) We introduce a novel multi-scale learning strategy for CVAE-based probabilistic models in order to make environment-aware collision-free trajectory predictions. (b) Unlike the prior works, we show that one can learn trajectory distributions that can be well generalized in new scenes at test time, giving various reasonable predictions compliant to the environment without needing extra steps for diversity. (c) The proposed coarse-to-fine approach enables diverse and accurate trajectory predictions by forecasting the heading of the entire trajectories through goal prediction and then expanding it to granular and complete predictions.

We demonstrate these contributions through experiments on both real and synthetic dataset. With various grounded evaluation metrics, we show that MUSE-VAE can produce predictions similar to GT trajectories while achieving less collision with the environment than the SOTA methods.

2. Related Work

The modeling of agent movement behavior, including individual humans, crowds, vehicles, etc., is a long-standing problem crossing the boundaries of multi-agent and computer vision communities. We focus on three relevant as-

pects: the forecasting of individual trajectories, the interplay between movement behavior and the environment, and the need for modeling that uncertainty in motion prediction.

Sequence Learning The human trajectory has a sequence characteristic that changes in turn according to the passage of time. In order to capture the nature of the sequential information, many prior works [1, 15, 25, 37, 38, 47] utilize Recurrent Neural Networks (RNNs) [32] such as LSTMs and GRUs. However, RNN suffers from forgetting the past hidden states as the recursion goes. [13, 50] tackle the temporal aspects of human trajectory forecasting by adopting Transformer Networks [46]. Transformer solves the long-range dependency problem by processing the a sequence as a whole with self-attention and positional encoding. Y-net [29] solves the sequential trajectory learning problem with only convolution layers. They represent trajectories with multiple heatmaps, which are stacked with the semantic environment map image along the channel dimension and fed to their convolution networks as a whole. This way, they learn temporal movements with the environment without tradition sequence learning networks.

Environment Learning A decision about the trajectory taken towards a goal depends on the surrounding environment. Many prior approaches provide environmental information to their model for realistic trajectory predictions. [37, 38, 50, 51] encode the environment layout and semantics as a representation of the scene image with a convolution network and use it to train their models along with trajectory features. While these approaches can learn the scene context surrounding the trajectory, they compress it into 1D feature vectors after CNNs and FCs layers, which can convey corrupted information in terms of spatial signals. Y-net [29] addresses this issue by aligning the semantic map with the trajectory heatmap spatially and processing them as a whole. Our model attempts more meaningful environmental learning without unnecessary information by focusing on a limited area around the trajectory rather than the entire scene while keeping the spatial signal by utilizing the heatmap trajectory representation.

Multimodal Learning The trajectory of an agent (human, vehicle, etc.) is affected by a number of factors such as the destination in mind, the surrounding environment, nearby agents and so on, which leads to an intrinsic uncertainty about the future behavior. Recent studies focus on learning the *distribution* of the human trajectory based on deep generative models, sidestepping the deterministic trajectory prediction. [19, 25, 38, 45, 50] adopt Conditional Variational AutoEncoders (CVAE) [40] and [15, 23, 37] introduce Generative Adversarial Network (GAN) [14] for learning of trajectory distribution where multiple predictions can be sampled. Trajectron++ [38] tackles the multimodal aspect of trajectory distributions by adopting a discrete latent distribution for the latent space, and Gaussian

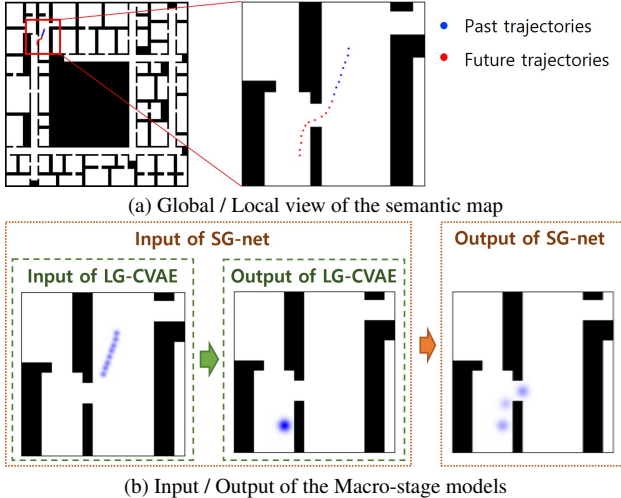


Figure 2. (a) The semantic map with 8 past / 12 future trajectories. Rather than the global map, we use the local map to focus on the nearby environment of the given trajectories. (b) Input and output format of Macro-stage models, LG-CVAE and SG-net. Trajectory heatmaps are overlaid with the local view semantic map. Here we assume 2 short-term goals at future time step 4 and 8 among 12 future steps. Thus, SG-net outputs 3 heatmaps; 2 for the short-term goals and 1 for the long-term goal.

Mixture Model as the output distribution of the decoder in their CVAE framework. AgentFormer [50] promotes diversity of the predictions with a pairwise distance loss across predictions. However, this approach requires retraining whenever a different number of predictions are sought at test time. Y-net [29] utilizes K-means clustering of predictive discrete density maps at test time to achieve diverse prediction; however, the model does not explicitly learn the resolution-free multimodal trajectory density. Some prior works [29, 33, 48, 51] encourage the multimodality by proposing a goal-conditioned forecasting model under the assumption that one’s movement depends primarily on the final goal position.

MUSE-VAE adopts a stage-wise training procedure to incorporate sequential information while maintaining a trajectory aligned with the environment. First, in the Macro-stage, future predictions are obtained by utilizing the heatmap representation of trajectories along with the semantic environment map, and then in the Micro-stage, RNN-based networks are used to facilitate sequence learning. The Micro-stage takes advantage of coarse predictions from the Macro-stage, reducing the long-range dependency problem and guiding the path to avoid obstacles. Adopting VAE in both Macro- and Micro-stages, our model learns the inherent uncertainty of forecasting, which can give a variety of plausible predictions.

3. Proposed Method

The trajectory prediction problem is formulated as follows. Assume that we are given $t_p > 0$ timestamps, the past trajectory positions $x = \{x_i^t\}_{t=1}^{t_p}$ of agent i in scene S , where $x_i^t \in \mathbb{R}^2$ denotes the 2D world coordinates of the agent i at time t . Our goal is to predict the future trajectory of the same agent during $t_f > 0$ future timestamps, $y = \{y_i^t\}_{t=t_p+1}^{t_p+f}$ in the sense of their distribution. $y_i^t \in \mathbb{R}^2$ is the future 2D position in the same coordinate system as x_i^t . This prediction should take into account the environmental context S , i.e., $p(y|x, S)$. We propose our Multi-Scale Environment-aware model, MUSE-VAE for coarse-to-fine trajectory forecasting. The Macro-stage is defined as a coarse prediction of the future trajectories, and the Micro-stage is defined as a fine prediction based on the coarse prediction. In the Macro-stage, only a subset of the future steps are predicted as the long-term and short-term goals. We denote the long-term goal as the final step at $t_{LG} = t_p+f$ and the short-term goals as some intermediate steps $t_{SG} \in \{t_{p+1}, \dots, t_{p+f-1}\}$. The Macro-stage aims to obtain rough predictions that are well aligned with the scene for collision avoidance against environmental obstacles. Based on the coarse prediction, the Micro-stage generates a fine-grained prediction of all t_f future steps. In this stage, we adopt the RNN [32] to efficiently learn the sequential features of trajectories.

In Sec. 3.1, we introduce the coarse prediction stage, Macro-stage, and elaborate on how the primary Macro-stage model, Long-term Goal Conditional VAE (LG-CVAE), and the subsequent Macro-stage model, Short-term Goal network (SG-net), are formulated. Sec. 3.2 introduces the Micro-stage, the fine prediction stage, used to refine predictions of complete forecast trajectories.

3.1. Macro-stage: Coarse Prediction Stage

One of the most important factors in the uncertainty of the future behavior is the future heading of an individual. One way to narrow the possibilities is to be aware of the surroundings and learn patterns from the past. [38, 50, 51] learn a representation of the environment, defined in image space, by encoding the semantic map of the scene into a 1D flattened feature, which can introduce distortion of spatial information of the scene. For alignment between trajectories and the semantic map, trajectories x are also represented in the pixel space as suggested in Y-net [29], using a Gaussian heatmap, denoted by I_x . The Gaussian filter has a variance of 4, and we create the homography matrices to map the world coordinates in meters to the image-based coordinates in pixel. All past trajectories are represented in one heatmap centered at the last observed position, while the long-term and short-term goal positions are created per location. Trajectories in t_p past timestamp are all represented in a sin-

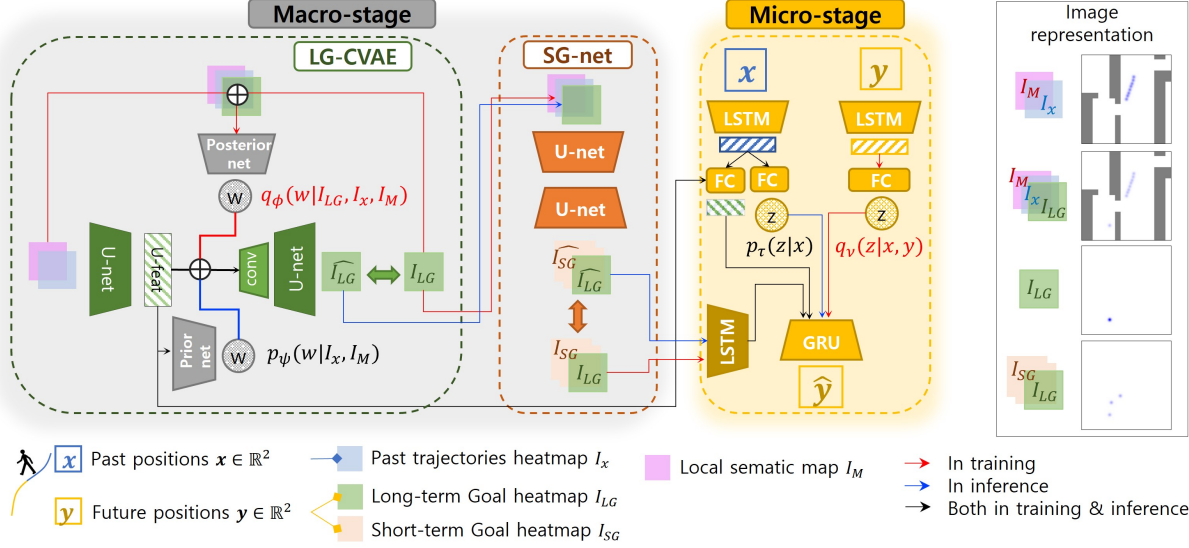


Figure 3. MUSE-VAE architecture. LG-CVAE is the first stage which predicts the long-term goal based on CVAE framework. Conditioned on the long-term goal, SG-net predicts the waypoints from the past trajectories to the long-term goal. We group these two stages as Macro-stage where the predictions are made in heatmap representation to keep the spatial signal along with the semantic map. Finally in Micro-stage, full trajectories are obtained with RNN-based CVAE. More implementation details are in the Supplementary Materials.

gle heatmap, while each future step is represented as one heatmap per step. The trajectory heatmap size matches the size of the semantic map.

Typically, the full environment information of a given scene is not necessary for long-term trajectory prediction. Often, the scene proximal to an agent’s current location is sufficient. Thus, we focus only on the local semantic map, with trajectory heatmaps created as illustrated in Fig. 2a. The local map is centered at the last observed agent location. The inputs and outputs of the Macro-stage are illustrated in Fig. 2b. The input of the long-term goal prediction model, LG-CVAE, consists of concatenated (local semantic map, past trajectory heatmap) and outputs one long-term goal heatmap. The short-term goal prediction model, SG-net, has the input of concatenated (local semantic map, past trajectory heatmap, long-term goal heatmap) and outputs $N_{SG} + 1$ heatmaps, where N_{SG} is the number of short-term goals¹. The local semantic map I_M can be determined as $f(S, x_i^{t_p}, \mathcal{H}, n)$ where f is the function that converts the global scene information S and homography \mathcal{H} into a local image-based representation of size (n, n) pixels centered at the last observed location $x_i^{t_p}$ of agent i .

3.1.1 LG-CVAE: Long-term Goal Prediction Model

Where a person will go in the future depends primarily on the long-term goal position. Therefore, for different potential future trajectories, it is of paramount importance to predict different long-term goal positions in good quality. To model the inherent uncertainty with semantic map and heatmap trajectory representations, we combine U-net [35]

and Conditional Variational AutoEncoder (CVAE) [40] as studied in [22]. Given the heatmap I_x of the past trajectories, the heatmap I_{LG} of the long-term goal, and the local semantic map I_M , the objective of the CVAE is to maximize the conditional distribution,

$$p(I_{LG}|I_x, I_M) = \int p_\theta(I_{LG}|w, I_x, I_M)p(w|I_x, I_M)dw. \quad (1)$$

The stochasticity of the conditional latent distribution $p(w|I_x, I_M)$ is propagated and contributes to the multimodality of $p(I_{LG}|I_x, I_M)$. The LG-CVAE loss is defined as the negative evidence lower bound as follows.

$$\mathcal{L}_{I_{LG}} = -\mathbb{E}_{q_\phi(w|I_{LG}, I_x, I_M)} [\log p_\theta(I_{LG}|w, I_x, I_M)] + KL(q_\phi(w|I_{LG}, I_x, I_M)||p_\psi(w|I_x, I_M)), \quad (2)$$

where $q_\phi(w|I_{LG}, I_x, I_M)$ and $p_\psi(w|I_x, I_M)$ are the posterior and the conditional prior distributions, respectively, assumed to be Gaussian for tractability. The output trajectory heatmap distribution $p_\theta(I_{LG}|w, I_x, I_M)$ has a Bernoulli distribution. Parameters of those densities are modeled using deep neural networks with the learning parameters ϕ , ψ , and θ , respectively, see Fig. 3. We use focal loss between the predicted heatmap $\widehat{I_{LG}}$ and the Ground Truth (GT) heatmap I_{LG} for the reconstruction loss to mitigate the imbalanced class issue in the trajectory heatmap representation.

Joint pixel-based environment-trajectory input (I_M, I_x) is encoded using a U-net architecture backbone [35], which shows excellent performance on semantic segmentation learning. The encoded U-net features of dimension (C, H, W) , where the feature map has C channels, a height

¹The extra count corresponds to the long-term goal.

of H , and a width of W , are average-pooled in the spatial dimension, and outputs $(C, 1, 1)$ feature maps, which are eventually converted to a C -dimensional vector. It is concatenated with the latent factor w sampled from the latent distribution. The posterior and the prior latent distributions are obtained from the separated posterior and prior network respectively consisting of convolutional layers.

To avoid the posterior collapse [4, 44] stemming from the strong U-net decoder, we pretrain the encoders and apply Free Bits [21] and KL annealing [5] strategies as studied in [26]. Additional implementation details are discussed in the Supplementary Materials.

3.1.2 SG-net: Short-term Goal Prediction Model

In the second stage of the Macro-stage, we predict the short-term goals based on the long-term goal prediction from LG-CVAE. The purpose of SG-net is to give waypoints from the last observed step to the long-term goal that are well-aligned with the environment. The final stage in Sec. 3.2 Micro-stage processes the trajectory and the semantic map as 1D feature vectors separately. Therefore, predicting all fine-grained future steps using only long-term goal information increases the risk of making predictions that are not well aligned with the environment based on destroyed spatial signals. SG-net utilizes U-net to generate $N_{SG} + 1$ heatmaps where N_{SG} is the number of short-term goals and 1 accounts for the long-term goal as illustrated in Fig. 2b. Unlike the LG-CVAE, this stage outputs the deterministic prediction based on the predicted long-term goal since we deal with the uncertainty of the fine trajectories other than long-term goals in the next stage. Thus, SG-net loss is simply reconstruction loss with focal loss as follows.

$$\mathcal{L}_{SG} = - \sum_{i=1}^{N_{SG}+1} (\alpha(1 - \widehat{I}_{SG_i})^\gamma I_{SG_i} \log(\widehat{I}_{SG_i}) + (1 - \alpha) \widehat{I}_{SG_i}^\gamma (1 - I_{SG_i}) \log(1 - \widehat{I}_{SG_i})), \quad (3)$$

where I_{SG} is the GT trajectory heatmap and \widehat{I}_{SG} is the predicted heatmap and $\alpha = 0.25, \gamma = 2$ as studied in [27].

3.2. Micro-stage: Fine Prediction Stage

In the final stage of our model, we predict complete future trajectories at the micro level. Here we change the coordinate from the discrete pixel coordinate to continuous world coordinate for fine predictions. Even if guided by predicted long-term and short-term goals from SG-net, individual steps may also have the variability stemming from the surrounding environment. To deal with this uncertainty, we leverage CVAE in this step as well. As illustrated in Fig. 3, we set $p(z|x)$ as the prior conditioned on past trajectories x , which is learned to approximate the posterior latent distribution $p(z|x, y)$ where y denotes the future trajectories. In test time, we sample the latent factor z from $p(z|x)$ to predict $p(y|z, x)$. While decoding future steps, our model use the long-term and short-term goal information from SG-net in the form of LSTM-encoded features.

We apply the Teacher Forcing technique to correct the prediction by feeding the GT/predicted long-term and short-term goals during training/test time respectively. To reduce the gap between training and test time reconstructions, we provide an additional reconstruction loss from the prior distribution following [7, 41]. Thus, Micro-stage training loss with β -weighted ELBO [17] is formulated as follows.

$$\mathcal{L}_{Micro} = -\mathbb{E}_{q_v(z|x, y)} [\log p_\eta(y|z, x)] - \mathbb{E}_{p_\tau(z|x)} [\log p_\eta(y|z, x)] + \beta KL(q_v(z|x, y) || p_\tau(z|x)), \quad (4)$$

where both the latent distributions and the output trajectory distribution are assumed as Gaussian distributions. We feed the U-net features from LG-CVAE to the prior network of Micro-stage so that the Micro-stage also recognizes the environment. Moreover, the Micro-stage encodes the GT/predicted I_{LG} and I_{SGs} with a bi-directional LSTM and feeds them to the decoder in training/test time respectively, which helps the fine predictions of each step.

4. Experiments

Sec. 4.1 introduces the datasets, evaluation metrics, and statistical analysis used in the experiments. Sec. 4.2 quantitatively evaluates SOTA models as well as MUSE-VAE. Sec. 4.3 compares the qualitative aspects of the predictions for intuitive assessment. In Sec. 4.4, each component of MUSE-VAE is analyzed by ablation studies.

4.1. Preliminaries

Datasets We used three datasets for the evaluation. The Stanford Drone Dataset (SDD) [34] is used in the TrajNet challenge [36] and prior works [29, 37]. The nuScenes Dataset [6] is a public autonomous driving dataset used by many prior arts [28, 31, 50]. In addition, we created a new Path Finding Simulation Dataset (PFS) using environments borrowed from [43]. Unlike SDD and nuScenes, the spaces in these environments are significantly more complex to navigate. For more details, please refer to the Supplementary Materials.

Evaluation Metrics For the evaluation, we adopted the standard metrics of minimum Average Displacement Error (ADE) and Final Displacement Error (FDE). We also report the Kernel Density Estimate-based Negative Log Likelihood (KDE NLL) used in [19, 38] as a comprehensive indicator of the predictive performance. Finally, we assess the Environment Collision-Free Likelihood (ECFL) [42], the probability that an agent has a path free of collision with the environment. We use it to address a drawback of existing works, which often neglect the importance of forecasting that adheres to environment structures. We report ECFL in percent points, where 100% means no collisions. More details can be found in the Supplementary Materials.

Statistical Analysis / Model Ranking It is challenging to compare different models across multiple metrics. Therefore, we test the statistical significance of the results, using

both traditional approach [9] and modern Bayesian analysis [2]. The Supplementary Materials provides the details.

4.2. Quantitative Results

We conduct experiments on the three datasets introduced in Sec. 4.1 and compare the performance of MUSE-VAE with Trajectron++ (T++) [38], Y-net [29], and AgentFormer (AF) [50] baselines, using their public code. Scene maps provided by PFSD and nuScenes show a much wider range of environments compared to SSD. Therefore, we provide a local view of the semantic map to all models including ours for a fair comparison. For all experiments in MUSE-VAE, we sample the latent factor z only once in Micro-stage, and we gain all diversity from the latent factor w in LG-CVAE by sampling it K times since we assume the uncertainty primarily depends on the long-term goal position.

Tab. 1 summarizes the experimental results on PFSD. Following the commonly used temporal horizon setting, we observe 3.2 sec (8 frames) and predict 4.8 sec (12 frames) future trajectories. Considering the increased complexity of the local environment layouts of PFSD, we choose sampling number $K = 20, 50$ to investigate the learned trajectory distribution. In ADE, our model can achieve the best performance in $K = 50$ and the second-best in $K = 20$. Although our model stands at second best in FDE, $K = 20$, it leads in KDE NLL and ECFL performance. The KDE NLL scores of Y-net and AF indicate that their K predictions fail to reflect the true trajectory distribution. This is because the K predictions are indirectly sampled from the learned distribution from their first training stage but sampled in the next stage by manipulating them to focus on the diversity. Y-net conducts a test time sampling trick based on K-means clustering to obtain diverse predictions. AF has the second stage training to apply the pairwise distance loss between K predictions for the diversity, which is inefficient since it requires re-training whenever K changes. On the other hand, MUSE-VAE can produce predictions within a low error range with GT trajectories, while reflecting the GT trajectory distribution (lower KDE NLL) and making realistic predictions reducing environment collisions (higher ECFL).

Tab. 2 shows the evaluation on SDD. It follows the same temporal horizon setup as PFSD. As in the prior works, we choose $K = 5, 20$ and errors are reported in pixel distance. MUSE-VAE can significantly outperform the state-of-the-art methods in ADE. Though our model shows the second best performance in FDE, MUSE-VAE largely ties up with the best method. For the same reason analyzed in PFSD, our model gives the best performance in KDE NLL. We can see that MUSE-VAE has slightly worse ECFL, which is still the second best, than Y-net. This is because the labeling of the scene provided from Y-net is incomplete², which adversely affects MUSE-VAE that relies heavily on the semantic map

²The incomplete labels are discussed in the Supplementary Materials.

Table 1. Results on the PFSD with $K = 20$ and 50. With $t_p = 3.2s$ (8 frames) and $t_f = 4.8s$ (12 frames), errors are in meters.

K	Model	ADE ↓	FDE ↓	KDE NLL ↓	ECFL ↑
20	T++	0.17	0.37	-0.88	83.32
	Y-net	0.13	0.20	0.20	91.52
	AF	0.08	0.11	0.47	94.54
	Ours	0.09	0.19	-1.66	97.40
50	T++	0.14	0.25	-1.11	83.39
	Y-net	0.09	0.12	0.04	91.74
	AF	0.08	0.09	1.17	95.37
	Ours	0.07	0.13	-1.94	97.50

Table 2. Results on the SDD with $K = 5$ and 20. With $t_p = 3.2s$ (8 frames) and $t_f = 4.8s$ (12 frames), errors are in pixels.

K	Model	ADE ↓	FDE ↓	KDE NLL ↓	ECFL ↑
5	T++	11.11	24.42	8.74	86.94
	Y-net	11.49	20.19	8.98	89.99
	AF	11.47	18.88	8.57	89.02
	Ours	9.60	19.70	8.43	89.30
20	T++	8.16	16.40	7.37	86.88
	Y-net	7.84	11.94	8.05	89.32
	AF	8.35	11.03	7.48	87.30
	Ours	6.36	11.10	7.21	89.30

Table 3. Results on the nuScenes with $K = 5$ and 10. With $t_p = 2s$ (4 frames) and $t_f = 6s$ (12 frames), errors are in meters.

K	Model	ADE ↓	FDE ↓	KDE NLL ↓	ECFL ↑
5	T++	3.14	7.45	7.20	68.99
	Y-net	2.46	5.15	11.03	85.46
	AF	1.59	3.14	9.39	86.74
	Ours	1.38	2.90	5.12	89.24
10	T++	2.46	5.65	5.61	69.02
	Y-net	1.88	3.47	7.52	82.90
	AF	1.30	2.47	7.76	85.76
	Ours	1.09	2.10	3.82	89.33

in Macro-stage predictions.

For the nuScenes dataset, following prior works, 2 sec (4 frames) observations and 6 sec (12 frames) predictions are made only for the vehicles and $K = 5, 10$ generations are investigated. Tab. 3 shows that our model consistently outperforms the others in every metric and sampling number. Compared to the previous two datasets, nuScenes has a longer future time horizon and all agents are vehicles, which makes the prediction length of trajectories much longer. On the other hand, since nuScenes is a real world dataset, many static past trajectories are also observed. Due to the fact that our model focuses on learning the trajectory distribution rather than simply having min ADE/FDE based on diverse samplings and generations, these real world data characteristics in nuScenes are well reflected in the trained model, which can lead to better performance across all metrics.

Statistical Analysis We computed average rankings of the methods, and T++, Y-Net, AF, and **Ours** obtain 3.42, 2.92, 2.33, **1.33**, respectively. We conducted the Friedman test [12] and confirmed that our method outperformed AF with statistical significance. We also conducted the Bayesian signed rank test [3] and confirmed that our method is either superior or at least on par versus the competitors. The Supplementary Materials explain this in further detail.

4.3. Qualitative Results

We provide additional qualitative context to the quantitative metrics, in order to reveal the underlying factors that support each model’s benefits and tradeoffs. In Fig. 4, we visualize several instances of predicted long and short-term goals as well as the trajectories in the context of different environments and movement behaviors, driven by the three datasets we used for evaluation. Specifically, Figs. 4a and 4b are instances from PFSD with $K = 20$, Figs. 4c and 4d are drawn for SDD with $K = 20$, and Figs. 4e and 4f come from nuScenes with $K = 10$. We take a look at instances of a ‘fork-in-the-road’ scenario from each dataset to test ability of models to understand the multimodality of long-term goals conditioned on the environment. In Figs. 4a, 4c and 4e, we overlay predicted trajectories and goal heatmaps from Macro-stage over local semantic maps to demonstrate the ability of the models to make reasonable coarse predictions in the context of different environment features. The first column with the green border is the long-term goal prediction from LG-CVAE. The following three columns with the orange border are two short-term goals and one long-term goal from SG-Net. The two rows show two different predictions generated by sampling two different latent factors w in LG-CVAE, based on the same observation x . We can see that (1) the short-term goals align well with the given predicted long-term goal, and (2) long-term goal projections naturally vary because of the structure of the ‘fork-in-the-road’ scenario, which gives a generally bimodal uncertainty in the possible goal directions.

Figs. 4b, 4d and 4f illustrate complete trajectory predictions, where the images in the clock-wise order, from the top-left, correspond to the Micro-stage of MUSE-VAE, followed by T++, AF, and Y-net, respectively. Across all three datasets, we can observe that predictions of T++ and AF tend to lead to collisions with the environment. On the other hand, predictions of Y-net and our MUSE-VAE are well-aligned and collision-free. We attribute this to T++ and AF encoding the semantic map into a 1D-representation, which entangles the spatial signal, while our model and Y-net process the semantic map along with the trajectory heatmap in 2D. Although Y-net produces predictions that avoid collision with obstacles, in contrast to MUSE-VAE it yields trajectories with diverse duration, which often overshoot or undershoot the true trajectory horizon. This is be-

Table 4. Ablation study on the PFSD with $K = 20$. With $t_p = 3.2s$ (8 frames) and $t_f = 4.8s$ (12 frames), errors are in meters.

Model	ADE ↓	FDE ↓	KDE NLL ↓	ECFL ↑
MUSE-VAE	0.09	0.19	-1.66	97.40
w/o SG-net	0.10	0.19	-1.39	97.27
w/o Micro-stage	0.10	0.20	-	99.75
w/o LL-prior	0.11	0.18	-1.77	95.06

cause the goal predictions of Y-net are not made directly by the learned model; rather, they stem from the test time sampling trick, which is weakly conditioned on the past trajectory signal, particularly its velocity. On the other hand, our MUSE-VAE’s goal predictions are not only well aligned with the environment structure in the Macro-stage, but also reflect learned dependency on the past trajectory sequence modeled by an RNN in the Micro stage.

4.4. Ablation Study

We analyze the effectiveness of each component in MUSE-VAE through an ablation study. Tab. 4 shows three ablated experiments in addition to the complete model MUSE-VAE. **w/o SG-net** model has no SG-net in Macro-stage, and thus, the long-term goal prediction is directly fed to the Micro-stage. **w/o Micro-stage** model does not include the Micro-stage, implying all future trajectories are predicted in the SG-net by letting $N_{SG} = t_f - 1$. In **w/o LL-prior** model, we eliminate the log-likelihood from the prior distribution $p_\tau(z|x)$ to assess the utility of this term in reducing the gap between the training and the inference-time reconstruction.

Our model requires the LG prediction produced by LG-CVAE, necessitating its presence in all experiments. LG-CVAE is also the primary factor influencing the variability of predictions. Thus, there is little observed variability in min ADE and min FDE. The most notable difference in performance stems from **w/o Micro-stage**, the absence of which precludes evaluation of the KDE NLL score. In this case, complete trajectory predictions happen in the SG-net, defined in discrete pixel coordinates, thus limiting the accuracy of the forecasted trajectory³. On the other hand, an advantage of this model is the few collisions, indicated by ECFL, because all predictions are obtained from pixel coordinates that are well aligned with the environment. In **w/o SG-net**, Micro-stage has no information of waypoints other than the long-term goal predictions from LG-CVAE. Thus, the KDE NLL values shows that distribution learning of **w/o SG-net** is not as good as a complete model. **w/o LL-prior** gives lower ECFL compared to other models. With reconstruction loss from the prior distribution during training, the model can learn how to produce predictions that better re-

³Complete trajectory predictions in this case are made from the heatmap maxima.

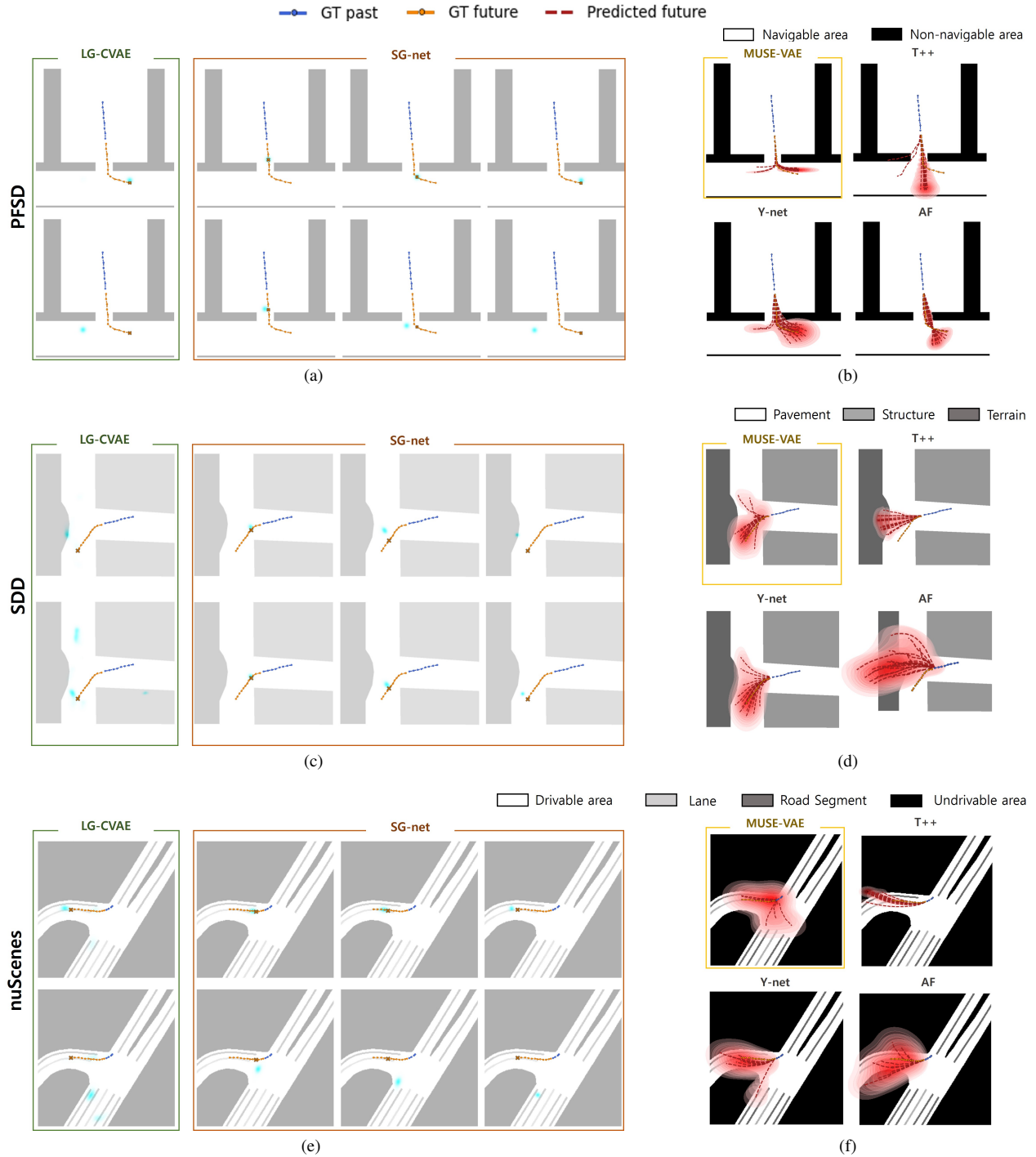


Figure 4. Left: Macro-stage results of (a) PFSD, (c) SDD, and (e) nuScenes respectively. In the first column, the Long-term Goal (LG) heat map prediction from LG-CVAE is overlaid on the local semantic map. The following three columns are two Short-term Goals (SG) and one LG from SG-Net. Here we show only two different sampling generations in each dataset. The blue and orange lines indicate GT past and GT future trajectories, respectively. GT LG and SGs are marked with ‘x’. Right: Complete trajectory predictions of (b) PFSD, (d) SDD, and (f) nuScenes respectively. In each dataset, the 1st/2nd/3rd/4th image from top-left to bottom-right is from Micro-stage of ours/Trajectron++/Y-net/AgentFormer, respectively. The blue, orange, and red lines indicate GT past, GT future, predicted future trajectories, respectively.

flect the length of the past trajectory, which results in predictions not deviating too much from the given scene map. This thorough ablation study shows that it is crucial to consider both the Macro-stage for coarse predictions aligned well with the environment and the Micro-stage for fine predictions reflecting the past sequential states.

5. Conclusion

In this paper, we introduce $MUSE-VAE$ a probabilistic model capable of recognizing the environment and generating multimodal predictions based on the coarse-to-fine approach. Our experimental results using various datasets and metrics show $MUSE-VAE$ achieves both versatile and accurate forecasts that are well matched to environmental conditions. $MUSE-VAE$ processes each agent independently, which cannot reflect agent-interaction. In the future work, we will take into consideration of multi agent-aware model that can avoid collisions with neighboring agents.

Supplementary Materials for MUSE-VAE

In this supplement, we provide additional details about the proposed MUSE-VAE, as well as the experimental evaluations, beyond those in the Main paper. [Appendix A](#) offers dataset specifications for SDD, nuScenes, and PFSD, with scene examples of each dataset. [Appendix B](#) elaborates on the implementation details, including the model networks and the approach we used to create the local view of the semantic map. In [Appendix C](#), we define the evaluation metrics used in the Main paper. [Appendix D](#) presents details of two statistical significance tests, the Friedman test used in the Main paper, and the Bayesian Signed Rank test, whose results are shown here. Both tests offer additional evidence in support of improvements that MUSE-VAE framework makes beyond the baseline models. [Appendix E](#) supplement the qualitative analyses in the Main paper, showcasing instances of scenarios and the predictions made by all models in those scenarios, to highlight the different effects those models have on the forecasting process. [Appendix F](#) shows the limitation of the SDD segmentation provided by Y-net [29] to explain the low ECFL discussed in [Sec. 4.2](#) of the Main paper. Finally, in [Appendix G](#), we discuss some key challenges of the trajectory prediction model and suggest possible directions for future research.

A. Datasets

A.1. Real World Datasets

The **Stanford Drone Dataset (SDD)** [34] consists of 20 unique scenes of college campus from bird-eye view collected by drones. It contains various agents such as pedestrians, cyclists, skateboarder, cart, car, and bus. We use the same split following the TrajNet challenge [36]. As in [29, 37], we sample at 2.5 Hz, which yields 3.2s (8 frames) observed trajectories and 4.8s (12 frames) future trajectories. We take advantage of the semantic map as well as the pixel data processed by [29]. The semantic segmentation map is labeled as 5 classes; pavement, road, structure, terrain, and tree where each class has the class ID 1, 2, 3, 4, and 5, respectively. A sample scene image and its semantic map from SDD is shown in [Fig. A.1a](#).

The **nuScenes Dataset** [6] is a public autonomous driving dataset. It provides 1,000 scenes in Boston, USA and Singapore and the corresponding HD semantic map with 11 annotated classes. Each scene is annotated at every 0.5s (2 Hz). Following the nuScenes prediction challenge setup, we split the train/val/test set, and predict only the vehicle category for 6s (12 frames) future trajectories based on 2s (4 frames) observations as in [28, 31, 50]. [Fig. A.1b](#) shows the global view of the binary map of the scene in Singapore with drivable (white-colored) area and undrivable (black-

colored) area that nuScenes dataset provides.

A.2. Synthetic Dataset

The **Path Finding Simulation Dataset (PFSD)** was generated by simulating the navigation of agents within 100 large synthetic environments borrowed from [43]. These environments were designed according to the external shapes and interior organizations of rooms and corridors generally found in contemporary architecture [10]. Unlike SDD and nuScenes, the non-navigable spaces in these environments are significantly more complex for navigation. Each of the environments was used to simulate 500 scenes (amounting to 50,000 total scenes), where a single agent navigates between two random points within the environment using the prevalent Social Force model [16]. As with SDD, the scenes were sampled at 2.5 Hz and further divided into training/val/test cases with 3.2s (8 frames) of observed trajectories and 4.8s (12 frames) of future trajectories. We use subset of the PFSD and make the train/val/test set with 40/2/4 different synthetic environments, respectively. We provide an environment example in [Fig. A.1c](#). It is the bi-

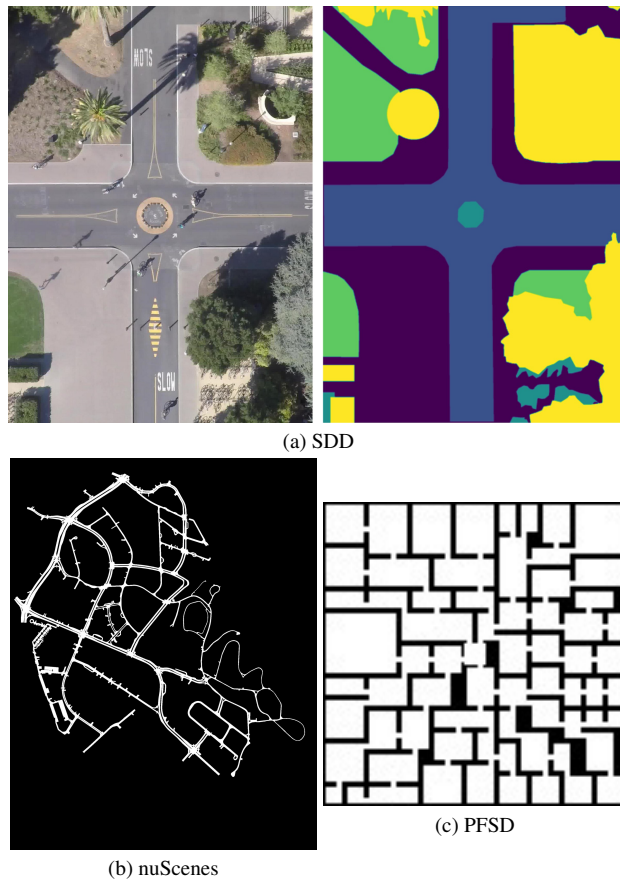


Figure A.1. (a) The global view of the scene image (left) and the semantic map (right). The global view of the semantic map of (b) nuScenes, (c) PFSD.

nary map consisting of navigable (white-colored) and non-navigable (black-colored) space of the entire environment of one scenario. An agent finds a path by moving from a room to another room using the exit between obstacles.

B. Implementation Details

B.1. Local Semantic Map

Stanford Drone Dataset (SDD)

We divide the semantic map class values (1 through 5) from Y-net [29] with 5 so that the class values become 0.2 (pavement), 0.4 (road), 0.6 (structure), 0.8 (terrain), 1 (tree). We center the local view of the semantic map at the last observed step. As real-world agents have varying lengths of trajectories, for the radius of the local map we compute the per-step traversed distance of all trajectories, in each sequence (20 frames), and set the radius to be 20 times larger than the per-step distance. Because the local semantic map is centered at the last observed position, it is possible that the local map region exceeds the original map. We represent those areas not in the original map as ‘non-navigable’ space. We assume ‘structure’ is the most non-navigable space among the five aforementioned classes, thus pad those areas with ‘structure’ class value. Each of the local map images and the Gaussian heatmaps for trajectories is resized into 256x256 pixels, then concatenated in the channel dimension.

nuScenes Dataset

We use the official code of AgentFormer [50] to preprocess the nuScenes semantic map. This results in a 3 channel semantic map with four categories: drivable area, lane, road segmentation, and undrivable area. We further preprocess this information to create a single-channel semantic map by setting the drivable area, lane, road segmentation, and undrivable area as 0, 0.3, 0.6, and 1, respectively. To determine a local map size, we use the same policy as in SDD. For the local map region out of the original map, we pad it with the ‘undrivable area’ class value.

Path Finding Simulation Dataset (PFSD)

Since the synthetic dataset has consistent step size throughout the data, we compute the average per-step distance across the entire training set, about 8-pixel distance. Based on this, the local view of the semantic map is centered at the last observed position of the agent and its size is 160×160 . We encode the navigable / non-navigable space as the values 0 / 1, respectively. The areas of the local map that deviate from the original map are padded by value 1 to indicate non-navigable space.

B.2. Networks

We implement MUSE-VAE in PyTorch. All networks are trained with Adam optimizer [20]. LG-CVAE has the backbone of U-net [35] combined with CVAE. U-net encoder

blocks consist of [32, 32, 64, 64, 64] output channel dimensions with the input channel 2 consisting of a local map and a heatmap for past trajectories. The decoder blocks have [64, 64, 64, 32, 32] output channel dimensions with the final output channel 1 to predict the long-term goal heatmap. The posterior network consists of convolutional layers with same output channels as the U-net encoder blocks. The prior network takes the feature from the U-net encoder and process it further using two convolutional layers with output channel dimension [32, 32]. Following [22], the resulting 2D feature map is average-pooled into 1x1, then fed to a 1x1 convolutional layer to estimate the mean and the standard deviation of the posterior and the prior latent distribution, with the dimension set to 10. To avoid the posterior collapse, the encoder of LG-CVAE is pretrained with the AE loss for 10 epochs with the learning rate of $1e^{-3}$. During training of LG-CVAE with VAE loss, we anneal the KL loss for the first 10 epochs; FB is set as 0.8, 6, and 3 for PFSD, SDD, and nuScenes, respectively. The learning rate is $1e^{-3}$, $1e^{-4}$, and $1e^{-4}$ for PFSD, SDD, and nuScenes, respectively.

SG-net is also based on the U-net. It has one additional block of 128 output channel dimensions more than LG-CVAE. The input channel of the encoder is 3, for a local map, a heatmap for past trajectories, and a heatmap for a long-term goal. The final output channel of the decoder is $N_{SG} + 1$ for N_{SG} heatmaps of N_{SG} short-term goals and a heatmap of a long-term goal. The learning rate is $1e^{-3}$, $1e^{-4}$, and $1e^{-3}$ for PFSD, SDD, and nuScenes, respectively.

In Micro-net, we utilize the position, velocity, and acceleration of the past sequence as in [38]. The prior network consists of an LSTM with 64 hidden dimensions and 2 FC layers with the output dimensions [256, 40] to estimate the mean (20D) and the standard deviation (20D) of the prior latent distribution. The 256 dimensional hidden feature from the prior network is processed once more by concatenating it with the feature from the LG-CVAE, which encodes the semantic map using FC layer with 32 output dimensions in order to give the map information to the decoder. The posterior network consists of a bi-directional LSTM with 64 hidden dimensions, followed by two FC layers with [256, 40] to estimate the mean (20D) and the standard deviation (20D) of the posterior latent distribution. The decoder has a GRU with 128 hidden dimensions, followed by FC layers to predict the mean and standard deviation of the 2D position distribution. The short-term goal heatmap predictions from Macro-stage are converted to the 2D position and encoded by bi-directional LSTM with 64 hidden dimensions and further processed into a 2D feature by FC layer and fed to the GRU. We use the learning rate $1e^{-3}$ and $\beta = 50$ for all datasets. FB is 0.07 for PFSD and nuScenes, and 1 for SDD.

A subset of our code for PFSD is provided as additional supplementary material. The complete code for MUSE-VAE will be released upon acceptance, following the conference policy.

C. Evaluation metrics

To evaluate the performance, we use four metrics: Average Displacement Error (ADE), Final Displacement Error (FDE), Kernel Density Estimate-based Negative Log Likelihood (KDE NLL), and Environment Collision-Free Likelihood (ECFL).

Average Displacement Error (ADE) Given t_f future timestamps, ADE is defined as the L_2 distance between the future GT and predictions which is averaged over t_f . Following prior works [1, 15, 19, 29, 38, 50], we report the minimum ADE among K ADEs obtained from K predictions.

Final Displacement Error (FDE) FDE is L_2 distance between the GT and prediction at the final future step t_{p+f} . Same as ADE, the minimum FDE among K predictions is reported.

Kernel Density Estimate-based Negative Log Likelihood (KDE NLL) To determine if the generative model learns the characteristics such as variance and multi-modality of the distribution, [19, 38] introduce KDE NLL. First, the pdf is estimated by Kernel Density Estimate (KDE) using the K sampled predictions at each future timestep, and then the mean log-likelihood of the GT trajectory is obtained based on the pdf. We adopt the approach in [38] and their publicly released code.

Environment Collision-Free Likelihood (ECFL) Realistic trajectory predictions should not violate environmental restrictions. [42] proposes ECFL, the probability an agent has a path that is free of collision with the environment defined as $ECFL(p, E) = \frac{1}{k} \sum_{i=1}^k \prod_{t=1}^{t_f} E[p_{i,t,0}, p_{i,t,1}]$, where E is the scene environment represented as a binary map with 1s and 0s indicating the navigable and the non-navigable spaces, respectively. p are the K predicted positions of an agent under the temporal horizon t_f . We report ECFL in percent points, where 100% means no collisions.

D. Statistical Validity Test

Since our evaluation used multiple datasets and four measures, we conducted additional analyses using the average rank [9] and the Bayesian statistical validity analysis [2] to assess the significance of the obtained results.

D.1. The Friedman Test

We borrow notations from [9] in this section. We first calculated the Friedman statistic [12] as

$$\chi_F^2 = \frac{12N}{k(k+1)} \left[\sum_j R_j^2 - \frac{k(k+1)^2}{4} \right], \quad (5)$$

where we compare k methods tested on N datasets. Here, R_j denotes the average ranks of algorithm j over all N datasets, i.e.,

$$R_j = \frac{1}{N} \sum_i r_i^j, \quad (6)$$

where r_i^j denotes the rank of j -th method among k algorithms tested on i -th dataset among N total datasets. One can approximate the probability distribution of the value as a Chi-square distribution. If k or N is small, one needs to find exact critical value from the precomputed table. Iman and Davenport [18] proposed a better statistic using the χ_F^2 ,

$$F_F = \frac{(N-1)\chi_F^2}{N(k-1) - \chi_F^2} \quad (7)$$

and this follows the F-distribution with $(k-1)$ and $(k-1)(N-1)$ degrees of freedom.

In our case, we have four methods to compare ($k=4$) and 24 datasets ($N=24$). We considered each evaluation setting (hyperparameter (K) choices, datasets, performance measures) as different datasets ($2 \times 3 \times 4$). Henceforth, we look for the F-distribution's critical value for 3 and 69 degrees of freedom. At 95% confidence level, the (upper) critical value is 2.737. Using the ranks obtained from our quantitative result, F_F is 21.278 which is significantly larger than the critical value, **rejecting the null hypothesis**, which states that all methods are equivalent.

As a post-hoc test, we conducted the Nemenyi test [30]. In the test, if two methods' average rank difference is larger than the critical difference defined as

$$CD = q_\alpha \sqrt{\frac{k(k+1)}{6N}}, \quad (8)$$

then there is a significant performance difference between the two methods. Here, q_α is 2.569 for $k=4$ at 95% confidence level, hence $CD = 0.957$. Since the average rank of our method is 1.33 and that of AF is 2.33, we argue that **our method outperformed AF** in the evaluation. Note that the average ranks of Y-Net and T++ are 2.92 and 3.42, respectively.

D.2. Bayesian Signed Rank Test

We also provide significance testing result based on modern Bayesian statistical validity analysis to address potential limitations of the traditional frequentist null hypothesis significance testing [2]. We ran the Bayesian signed-rank test [3] for each pair of methods and for each measure. This test also accounts for the region of practical equivalence (ROPE) [24]. If the difference between two methods is smaller than the ROPE, then there is no practical difference in performance.

In our evaluation, we have several metrics and datasets and each needs a careful definition of ROPE to conduct a proper analysis. First, for ADE and FDE, we adopted the standard 0.5 meter difference as the ROPE [38]. However, one of the datasets we used, SDD, does not have the geometric calibration data to obtain metered measures in its test set, unlike PFSD and nuScenes. Henceforth, prior works, e.g., [29], used pixel differences to calculate the ADE and FDE. Therefore, we used 1 pixel difference for the ROPE, considering the resolution of the image and approximate sizes of real world structures and objects in the scene. It should be noted that, we also tested with a larger ROPE (3 pixels), but there was no change in the conclusion of this analysis. For KDE NLL, it is challenging to define ROPE since NLL is not a scale, but a likelihood value. So we set ROPE as zero for NLL. For ECFL, since it has same scale as accuracy [0, 100], we use the standard 1% difference for the ROPE.

In Tabs. D.1 to D.4, we report the Bayesian signed-rank pairwise test result for $C(4, 2) = 6$ comparisons. Tab. D.5 summarizes all the aforementioned pairwise results by computing the average ranks of each method, in each of the tables Tabs. D.1 to D.4, based on the number of times the method "won", "tied", or "lost" in the pairwise comparison. For instance, in Tab. D.3, MUSE-VAE won 3-out-of-6 times, T++ 2/6, AF 1/6, and Y-Net 0/6 times, resulting in ranks of 1, 2, 3, and 4 for the four methods, respectively. Based on this, and in line with the traditional frequentist analysis in Sec. D.1, we conclude that **our MUSE-VAE outperforms the SOTA competitors**, on average, across all datasets and measures.

E. Additional Qualitative Evaluations

Fig. E.1 shows qualitative results in the same manner as those presented in Fig. 4 of the Main paper. Here we investigate several key scenarios from each dataset, beyond the 'fork-in-the-road' introduced in Fig. 4. Scenarios were selected to highlight the challenges all models face in forecasting the environment-aware trajectories and offer insights into how the models behave when faced with environment constraints, in order to reveal the models' benefits and downsides.

The difference in the environment configurations between the two PFSD instances, Fig. E.1b here and Fig. 4b in the Main paper, is that Fig. E.1b has no obstacles in the direction of the observed, past trajectory while Fig. 4b presents obstacles at the bottom of the map in the same direction. Thus, comparing the predictions, our method predicted both straight ahead and left or right curved trajectories for Fig. E.1b, while producing only left or right curves for Fig. 4b.

Fig. E.1d shows an example when the ground truth trajectory passes right next to the 'structure' area, which is

Table D.1. Comparing ADE of methods using Bayesian signed-rank test. For PFSD and nuScenes, ROPE is defined as 0.5 meters. For SDD, ROPE is 1 pixel.

PFSD, nuScenes				
Method A	p(A > B)	p(A ≈ B)	p(A < B)	Method B
T++	0.00	0.87	0.13	Y-Net
T++	0.00	0.27	0.73	AF
T++	0.00	0.27	0.73	Ours
Y-Net	0.00	0.87	0.13	AF
Y-Net	0.00	0.59	0.41	Ours
AF	0.00	1.00	0.00	Ours
SDD				
Method A	p(A > B)	p(A ≈ B)	p(A < B)	Method B
T++	0.00	1.00	0.00	Y-Net
T++	0.00	1.00	0.00	AF
T++	0.00	0.27	0.73	Ours
Y-Net	0.00	1.00	0.00	AF
Y-Net	0.00	0.27	0.73	Ours
AF	0.00	0.27	0.73	Ours

Table D.2. Comparing FDE of methods using Bayesian signed-rank test. For PFSD and nuScenes, ROPE is defined as 0.5 meters. For SDD, ROPE is 1 pixel.

PFSD, nuScenes				
Method A	p(A > B)	p(A ≈ B)	p(A < B)	Method B
T++	0.00	0.27	0.73	Y-Net
T++	0.00	0.27	0.73	AF
T++	0.00	0.27	0.73	Ours
Y-Net	0.00	0.43	0.57	AF
Y-Net	0.00	0.27	0.73	Ours
AF	0.00	1.00	0.00	Ours
SDD				
Method A	p(A > B)	p(A ≈ B)	p(A < B)	Method B
T++	0.00	0.04	0.96	Y-Net
T++	0.00	0.04	0.96	AF
T++	0.00	0.04	0.96	Ours
Y-Net	0.00	0.56	0.44	AF
Y-Net	0.00	1.00	0.00	Ours
AF	0.00	1.00	0.00	Ours

non-navigable; the heading direction is mostly blocked by the structure. Our model can make predictions that do not violate the environmental constraints, going back or turning left to search for navigable space. On the other hand, the predictions from the baseline models collide with the obstacles, a violation of the desired behavior.

Fig. E.1f is a fork-in-the-road scenario like Fig. 4f, with another drivable area on the other side of the fork in the

Table D.3. Comparing KDE NLL of methods using Bayesian signed-rank test. ROPE is 0 in this case.

Method A	p(A > B)	p(A ≈ B)	p(A < B)	Method B
T++	1.00	0.00	0.00	Y-Net
T++	0.99	0.00	0.01	AF
T++	0.00	0.00	1.00	Ours
Y-Net	0.31	0.00	0.69	AF
Y-Net	0.00	0.00	1.00	Ours
AF	0.00	0.00	1.00	Ours

Table D.4. Comparing ECFL of methods using Bayesian signed-rank test. ROPE is 1%.

Method A	p(A > B)	p(A ≈ B)	p(A < B)	Method B
T++	0.00	0.00	1.00	Y-Net
T++	0.00	0.00	1.00	AF
T++	0.00	0.00	1.00	Ours
Y-Net	0.02	0.27	0.70	AF
Y-Net	0.00	0.04	0.96	Ours
AF	0.00	0.01	0.99	Ours

Table D.5. Average rank of the four contrasted approaches, based on the Bayesian Signed Rank pairwise test results in Tabs. D.1 to D.4, across all measures.

Method	Average Rank of Bayesian Test Results
T++	3.50
Y-net	3.00
AF	2.16
Ours	1.33

road. Although the traffic flow in this area is in the direction opposite to the predicted trajectory, it still is a drivable area. Since we have never provided a clear guidance for learning in which direction to drive based on the ‘correct’ lane, our model simply treats this area as drivable and makes one possible prediction. It can be seen that the baseline models cannot consider this possibility, instead making many predictions into the undrivable area.

Finally, Tab. E.1 shows the corresponding quantitative results for each dataset with metrics introduced in Appendix C. The results in the table are well-aligned with the visualization in the Tab. E.1. MUSE-VAE shows the highest ECFL in all datasets, suggesting our model forecasts environmentally-compliant trajectories. Moreover, our model shows the best performance for all datasets in terms of ADE; it similarly leads in FDE performance in SDD and nuScenes. MUSE-VAE attains the second best results in FDE for PFSD, trailing the top Y-Net by only 0.01 meter. Similarly, MUSE-VAE approaches the top method (AF) in KDE NLL for nuScenes. The third ranked performance of our model in KDE NLL of SDD stems from

Table E.1. Quantitative results of Fig. E.1. PFSD and SDD with $t_p = 3.2s$ (8 frames) and $t_f = 4.8s$ (12 frames), and nuScenes with $t_p = 2s$ (4 frames) and $t_f = 6s$ (12 frames). Errors are in meters for PFSD and nuScenes, and in pixels for SDD.

Dataset	Model	ADE ↓	FDE ↓	KDE NLL ↓	ECFL ↑
PFSD (K = 20)	T++	0.16	0.05	-1.54	95
	Y-net	0.1	0.04	-0.76	100
	AF	0.12	0.05	-0.50	100
	Ours	0.08	0.05	-4.24	100
SDD (K = 20)	T++	4.15	3.18	6.58	80
	Y-net	3.15	2.88	7.77	65
	AF	13.44	7.10	8.69	20
	Ours	2.86	2.34	8.45	100
nuScenes (K = 10)	T++	4.92	4.91	3.91	0
	Y-net	3.08	2.99	6.21	40
	AF	1.17	1.08	3.68	30
	Ours	0.89	0.73	3.84	90

those predictions heading to the left or going back toward the past trajectories. While away from the specific trajectory taken by the agent in this instance, the behaviors predicted by MUSE-VAE are very reasonable strategies for an agent who reaches a dead-end.

F. Limitation of SDD Segmentation

In our evaluations, we used the semantic map of SDD provided by Y-net. They classify the scene environment into the five classes described in Appendix B. In Fig. F.1, we show SDD scene images and their semantic maps of the scene (a) coupa_0 and (b) little_3. Red points indicate all trajectories in each scene.

There are two major problems in learning this map. First, it is not clear which semantic classes ought to be considered as navigable. Based on the class names, only pavement and road may be reasonably navigable space, but as seen in Fig. F.1, there are trajectories on tree, terrain, and structure. For the evaluation, we set only the ‘structure’ class as the obstacle class. Secondly, the segmentation regions are semantically inaccurate. Near the bottom-center of the semantic map of Fig. F.1a, we can see the squares all colored in yellow, which indicates a tree. However, looking at the scene image, we notice that not all of those regions are trees.

These inaccurate annotations give rise to the model confusion on how to deal with the map information when determining the trajectories that should only exist in navigable spaces. This affects MUSE-VAE more significantly than other models since the decision of long-term and short-term goals in Macro-stage heavily depend on the local map information; this subsequently leads to slightly lower ECFL for SDD in Sec. 4.2 of the Main paper, compared to other approaches.

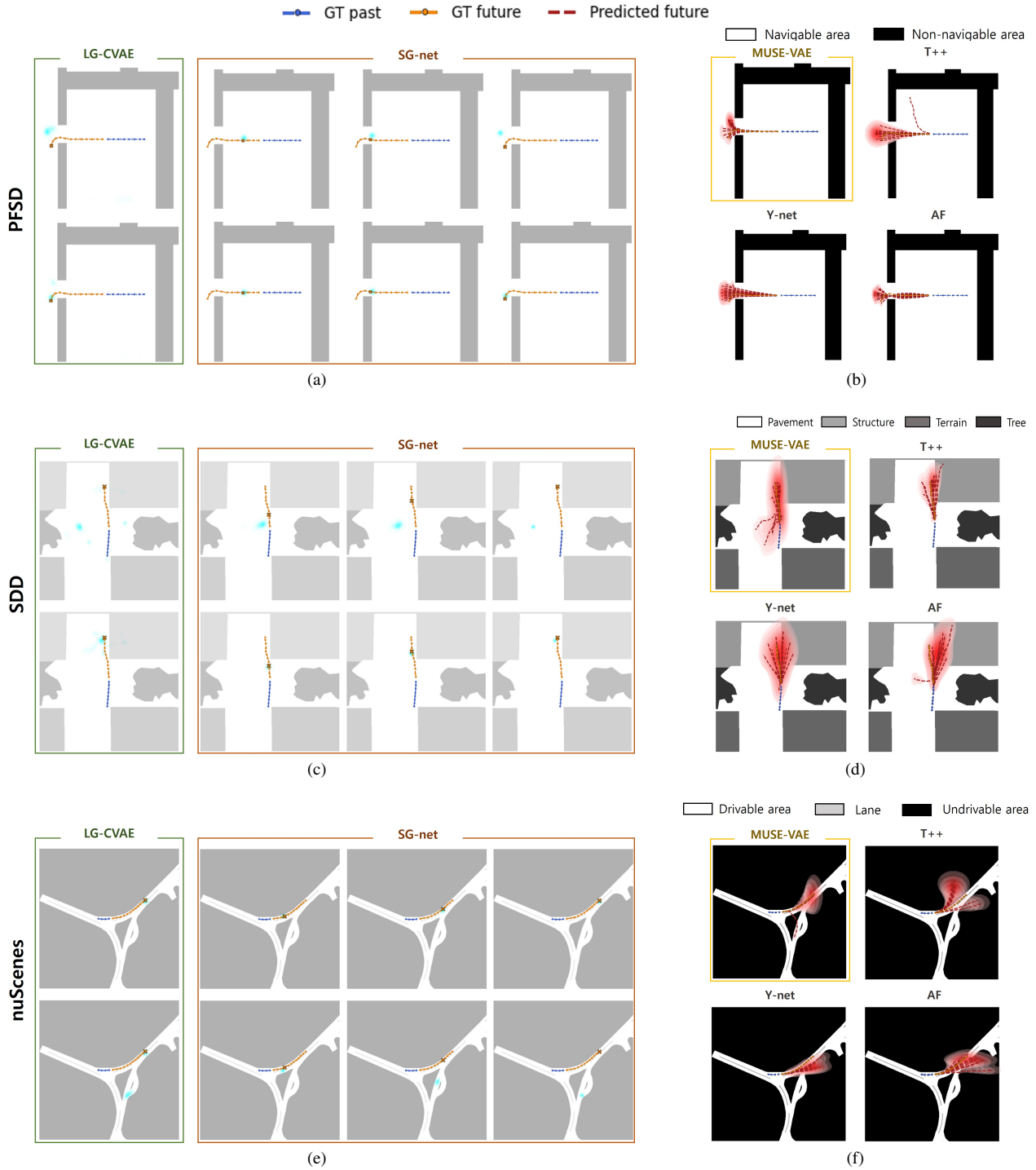
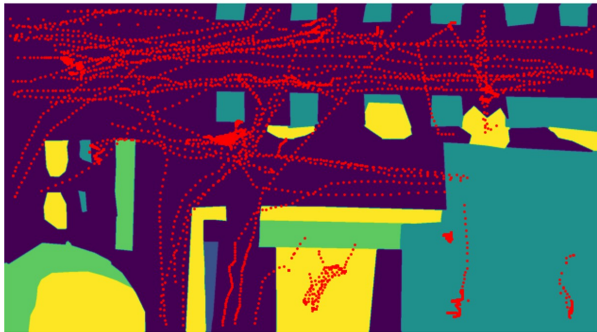
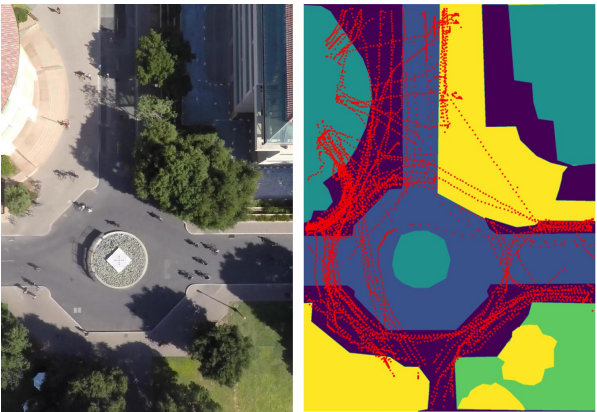


Figure E.1. Left: Macro-stage results of (a) PFSD, (c) SDD, and (e) nuScenes respectively. In the first column, the Long-term Goal (LG) heat map prediction from LG-CVAE is overlaid on the local semantic map. The following three columns are two Short-term Goals (SG) and one LG from SG-Net. Here we show only two different sampling generations in each dataset. The blue and orange lines indicate GT past and GT future trajectories, respectively. GT LG and SGs are marked with 'x'. Right: Complete trajectory predictions of (b) PFSD, (d) SDD, and (f) nuScenes respectively. In each dataset, the 1st/2nd/3rd/4th image from top-left to bottom-right is from Micro-stage of ours/Trajnet++/Y-net/AgentFormer, respectively. The blue, orange, and red lines indicate GT past, GT future, predicted future trajectories, respectively.

Pavement
 Road
 Structure
 Terrain
 Tree



(a) coupa_0



(b) little_3

Figure F.1. SDD scene image and its semantic map of the scene (a) coupa_0 and (b) little_3. Red points indicate all trajectories in each scene. Trajectories are found in the region with classes like ‘structure’ or ‘tree’, which is unexpected in terms of navigability.

G. Challenges and Future Work

In this paper, we proposed to “boost” the learning of models that forecast realistic, environment-aware trajectories by leveraging the large body of scene-compliant simulated trajectories in PFSD, a complex environment with intricate navigable / non-navigable structures. These structures were designed to induce diverse agent-environment behaviors, hence data to train models, that generalize well to many real-world scenarios.

Another component that makes trajectory prediction realistic is the absence of collisions among the agents them-

selves. One way to learn models that accomplish this, aside from collecting large bodies of real-world data, is to create synthetic datasets that reflect the desired agent-agent relationships, much like PFSD captures the environment-agent interactions. Such trained models would then transfer to the (smaller) real world datasets.

However, synthesizing collision-free models for agent-agent interactions is a challenging task. While designing scenarios where only the inter-agent distance is kept above a certain threshold is possible, such instances directly eliminate more complex yet desired behaviors such as agents walking together as a group or agents passing by each other in the opposite directions. Moreover, the behavioral patterns determining inter-agent proximity are also contextualized by the surrounding environment. For instance, the density of agents (hence their mutual displacements), will be higher (displacements lower) in very narrow navigable spaces compared to those in wider, open environments.

We leave it as an open research challenge to study such integrated models that can consider the inter-agent relationship in addition to the agent-environment interactions we tackled here using our MUSE-VAE.

References

- [1] Alexandre Alahi, Kratharth Goel, Vignesh Ramanathan, Alexandre Robicquet, Li Fei-Fei, and Silvio Savarese. Social lstm: Human trajectory prediction in crowded spaces. In *2016 IEEE Conference on Computer Vision and Pattern Recognition (CVPR)*, pages 961–971, 2016. 2, 3
- [2] Alessio Benavoli, Giorgio Corani, Janez Demšar, and Marco Zaffalon. Time for a change: a tutorial for comparing multiple classifiers through bayesian analysis. *Journal of Machine Learning Research*, 18(77):1–36, 2017. 6, 3
- [3] A. Benavoli, F. Mangili, G. Corani, M. Zaffalon, and F. Ruggeri. A bayesian wilcoxon signed-rank test based on the dirichlet process. In *Proceedings of the 31st International Conference on International Conference on Machine Learning - Volume 32, ICML'14*, page II–1026–II–1034. JMLR.org, 2014. 7, 3
- [4] Samuel R. Bowman, Gabor Angeli, Christopher Potts, and Christopher D. Manning. A large annotated corpus for learning natural language inference. In *EMNLP*, 2015. 5
- [5] Samuel R. Bowman, Luke Vilnis, Oriol Vinyals, Andrew M. Dai, Rafal Józefowicz, and Samy Bengio. Generating sentences from a continuous space. In *CoNLL*, 2016. 5
- [6] Holger Caesar, Varun Bankiti, Alex H. Lang, Sourabh Vora, Venice Erin Liong, Qiang Xu, Anush Krishnan, Yu Pan, Giancarlo Baldan, and Oscar Beijbom. nuscenes: A multimodal dataset for autonomous driving. *2020 IEEE/CVF International Conference on Computer Vision and Pattern Recognition (CVPR)*, pages 11618–11628, 2020. 1, 5
- [7] Yujun Cai, Yiwei Wang, Yi-Hao Zhu, T. Cham, Jianfei Cai, Junsong Yuan, Jun Liu, Chuanxia Zheng, Sijie Yan, Henghui Ding, Xiaohui Shen, Ding Liu, and Nadia Magnenat Thalmann. A unified 3d human motion synthesis model via conditional variational auto-encoder. 2021. 5
- [8] Eric Chown, Stephen Kaplan, and David Kortenkamp. Prototypes, location, and associative networks (plan): Towards a unified theory of cognitive mapping. *Cognitive Science*, 19(1):1–51, 1995. 2
- [9] Janez Demšar. Statistical comparisons of classifiers over multiple data sets. *Journal of Machine Learning Research*, 7(1):1–30, 2006. 6, 3
- [10] Timur Dogan, Emmanouil Saratsis, and Christoph Reinhart. The optimization potential of floor-plan typologies in early design energy modeling. 2015. 1
- [11] Gonzalo Ferrer, Anais Garrell, and Alberto Sanfeliu. Social-aware robot navigation in urban environments. In *2013 European Conference on Mobile Robots*, pages 331–336. IEEE, 2013. 1
- [12] Milton Friedman. The use of ranks to avoid the assumption of normality implicit in the analysis of variance. *Journal of the American Statistical Association*, 32(200):675–701, 1937. 7, 3
- [13] Francesco Giuliari, Irtiza Hasan, Marco Cristani, and Fabio Galasso. Transformer networks for trajectory forecasting. *2020 25th International Conference on Pattern Recognition (ICPR)*, pages 10335–10342, 2021. 2
- [14] Ian J. Goodfellow, Jean Pouget-Abadie, Mehdi Mirza, Bing Xu, David Warde-Farley, Sherjil Ozair, Aaron C. Courville, and Yoshua Bengio. Generative adversarial nets. In *NIPS*, 2014. 2
- [15] Agrim Gupta, Justin Johnson, Li Fei-Fei, Silvio Savarese, and Alexandre Alahi. Social gan: Socially acceptable trajectories with generative adversarial networks. pages 2255–2264, 06 2018. 1, 2, 3
- [16] Dirk Helbing and Peter Molnar. Social Force Model for Pedestrian Dynamics. *Physical review E*, 51(5):4282, 1995. 1
- [17] Irina Higgins, Loic Matthey, Arka Pal, Christopher P. Burgess, Xavier Glorot, Matthew M. Botvinick, Shakir Mohamed, and Alexander Lerchner. beta-vae: Learning basic visual concepts with a constrained variational framework. In *ICLR*, 2017. 5
- [18] Ronald L. Iman and James M. Davenport. Approximations of the critical region of the friedman statistic. *Communications in Statistics - Theory and Methods*, 9(6):571–595, 1980. 3
- [19] B. Ivanovic and Marco Pavone. The trajectron: Probabilistic multi-agent trajectory modeling with dynamic spatiotemporal graphs. *2019 IEEE/CVF International Conference on Computer Vision (ICCV)*, pages 2375–2384, 2019. 2, 5, 3
- [20] Diederik P. Kingma and Jimmy Ba. Adam: A method for stochastic optimization. In Yoshua Bengio and Yann LeCun, editors, *3rd International Conference on Learning Representations, ICLR 2015, San Diego, CA, USA, May 7-9, 2015, Conference Track Proceedings*, 2015. 2
- [21] Diederik P. Kingma, Tim Salimans, and Max Welling. Improved variational inference with inverse autoregressive flow. *ArXiv*, abs/1606.04934, 2017. 5
- [22] Simon A. A. Kohl, Bernardino Romera-Paredes, Clemens Meyer, Jeffrey De Fauw, Joseph R. Ledsam, Klaus Maier-Hein, S. M. Ali Eslami, Danilo Jimenez Rezende, and Olaf Ronneberger. A probabilistic u-net for segmentation of ambiguous images. In *NeurIPS*, 2018. 4, 2
- [23] Vineet Kosaraju, Amir Sadeghian, Roberto Martín-Martín, Ian D. Reid, Seyed Hamid Rezatofighi, and Silvio Savarese. Social-bigat: Multimodal trajectory forecasting using bicycle-gan and graph attention networks. In *NeurIPS*, 2019. 2
- [24] John K. Kruschke and Torrin M. Liddell. The bayesian new statistics: Hypothesis testing, estimation, meta-analysis, and power analysis from a bayesian perspective. *Psychonomic Bulletin & Review*, 25(1):178–206, Feb 2018. 3
- [25] Namhoon Lee, Wongun Choi, Paul Vernaza, Christopher Bongsoo Choy, Philip H. S. Torr, and Manmohan Chandraker. Desire: Distant future prediction in dynamic scenes with interacting agents. *2017 IEEE Conference on Computer Vision and Pattern Recognition (CVPR)*, pages 2165–2174, 2017. 2
- [26] Bohan Li, Junxian He, Graham Neubig, Taylor Berg-Kirkpatrick, and Yiming Yang. A surprisingly effective fix for deep latent variable modeling of text. In *Conference on Empirical Methods in Natural Language Processing (EMNLP)*, Hong Kong, November 2019. 5
- [27] Tsung-Yi Lin, Priya Goyal, Ross B. Girshick, Kaiming He, and Piotr Dollár. Focal loss for dense object detection. 2017

- IEEE International Conference on Computer Vision (ICCV)*, pages 2999–3007, 2017. [5](#)
- [28] Yecheng Jason Ma, Jeevana Priya Inala, Dinesh Jayaraman, and Osbert Bastani. Diverse sampling for normalizing flow based trajectory forecasting. *ArXiv*, abs/2011.15084, 2020. [5](#), [1](#)
- [29] Karttikeya Mangalam, Yang An, Harshayu Girase, and Jitendra Malik. From goals, waypoints & paths to long term human trajectory forecasting. In *Proc. International Conference on Computer Vision (ICCV)*, Oct. 2021. [2](#), [3](#), [5](#), [6](#), [1](#), [4](#)
- [30] Peter B. Nemenyi. *Distribution-Free Multiple Comparisons*. PhD thesis, Princeton University, 1963. [3](#)
- [31] Tung Phan-Minh, Elena Corina Grigore, Freddy A. Boulton, Oscar Beijbom, and Eric M. Wolff. Covernet: Multimodal behavior prediction using trajectory sets. *2020 IEEE/CVF Conference on Computer Vision and Pattern Recognition (CVPR)*, pages 14062–14071, 2020. [5](#), [1](#)
- [32] Bastiaan Quast. rnn: a recurrent neural network in r. *Working Papers*, 2016. [2](#), [3](#)
- [33] Nicholas Rhinehart, Rowan McAllister, Kris Kitani, and Sergey Levine. Precog: Prediction conditioned on goals in visual multi-agent settings. *2019 IEEE/CVF International Conference on Computer Vision (ICCV)*, pages 2821–2830, 2019. [3](#)
- [34] Alexandre Robicquet, Amir Sadeghian, Alexandre Alahi, and Silvio Savarese. Learning social etiquette: Human trajectory understanding in crowded scenes. In *ECCV*, 2016. [5](#), [1](#)
- [35] Olaf Ronneberger, Philipp Fischer, and Thomas Brox. U-net: Convolutional networks for biomedical image segmentation. volume 9351, pages 234–241, 10 2015. [4](#), [2](#)
- [36] Amir Sadeghian, Vineet Kosaraju, Agrim Gupta, Silvio Savarese, and A Alahi. Trajnet: Towards a benchmark for human trajectory prediction. *arXiv preprint*, 2018. [5](#), [1](#)
- [37] Amir Sadeghian, Vineet Kosaraju, Ali Sadeghian, Noriaki Hirose, Hamid Rezatofighi, and Silvio Savarese. Sophie: An attentive gan for predicting paths compliant to social and physical constraints. pages 1349–1358, 06 2019. [2](#), [5](#), [1](#)
- [38] Tim Salzmann, Boris Ivanovic, Punarjay Chakravarty, and Marco Pavone. *Trajectron++: Dynamically-Feasible Trajectory Forecasting with Heterogeneous Data*, pages 683–700. 12 2020. [2](#), [3](#), [5](#), [6](#), [4](#)
- [39] Farnaz Sharif, Behnam Tayebi, György Buzsáki, Sebastien Royer, and Antonio Fernandez-Ruiz. Subcircuits of deep and superficial cal place cells support efficient spatial coding across heterogeneous environments. *Neuron*, 109(2):363–376, 2021. [2](#)
- [40] Kihyuk Sohn, Honglak Lee, and Xinchen Yan. Learning Structured Output Representation using Deep Conditional Generative Models. In *Neural Information Processing Systems (NIPS)*, 2015. [2](#), [4](#)
- [41] Kihyuk Sohn, Honglak Lee, and Xinchen Yan. Learning structured output representation using deep conditional generative models. In *NIPS*, 2015. [5](#)
- [42] Samuel S. Sohn, Mihee Lee, Seonghyeon Moon, Gang Qiao, Muhammad Usman, Sejong Yoon, Vladimir Pavlovic, and Mubbasir Kapadia. A2x: An agent and environment interaction benchmark for multimodal human trajectory prediction. In *Motion, Interaction and Games, MIG '21*, New York, NY, USA, 2021. Association for Computing Machinery. [5](#), [3](#)
- [43] Samuel S Sohn, Honglu Zhou, Seonghyeon Moon, Sejong Yoon, Vladimir Pavlovic, and Mubbasir Kapadia. Laying the foundations of deep long-term crowd flow prediction. In *European Conference on Computer Vision*, pages 711–728. Springer, 2020. [5](#), [1](#)
- [44] Casper Kaae Sønderby, Tapani Raiko, Lars Maaløe, Søren Kaae Sønderby, and Ole Winther. Ladder variational autoencoders. In *NIPS*, 2016. [5](#)
- [45] Yichuan Tang and Ruslan Salakhutdinov. Multiple futures prediction. In *NeurIPS*, 2019. [2](#)
- [46] Ashish Vaswani, Noam Shazeer, Niki Parmar, Jakob Uszkoreit, Llion Jones, Aidan N. Gomez, Łukasz Kaiser, and Illia Polosukhin. Attention is all you need. In *Proceedings of the 31st International Conference on Neural Information Processing Systems, NIPS'17*, page 6000–6010, Red Hook, NY, USA, 2017. Curran Associates Inc. [2](#)
- [47] Anirudh Vemula, Katharina Muelling, and Jean Oh. Social attention: Modeling attention in human crowds. *2018 IEEE International Conference on Robotics and Automation (ICRA)*, pages 1–7, 2018. [2](#)
- [48] Chuhua Wang, Yuchen Wang, Mingze Xu, and David J. Crandall. Stepwise goal-driven networks for trajectory prediction. *ArXiv*, abs/2103.14107, 2021. [2](#), [3](#)
- [49] Jan M Wiener, Simon J Büchner, and Christoph Hölscher. Taxonomy of human wayfinding tasks: A knowledge-based approach. *Spatial Cognition & Computation*, 9(2):152–165, 2009. [1](#)
- [50] Ye Yuan, Xinshuo Weng, Yanglan Ou, and Kris Kitani. Agentformer: Agent-aware transformers for socio-temporal multi-agent forecasting. In *Proceedings of the IEEE/CVF International Conference on Computer Vision (ICCV)*, 2021. [2](#), [3](#), [5](#), [6](#), [1](#)
- [51] Hang Zhao, Jiyang Gao, Tian Lan, Chen Sun, Benjamin Sapp, Balakrishnan Varadarajan, Yue Shen, Yi Shen, Yunqing Chai, Cordelia Schmid, Congcong Li, and Dragomir Anguelov. TNT: target-driven trajectory prediction. *CoRR*, abs/2008.08294, 2020. [2](#), [3](#)